

Separation of Iron Phase and P-Bearing Slag Phase from Gaseous-Reduced, High-Phosphorous Oolitic Iron Ore at 1473 K (1200 °C) by Super Gravity



JINTAO GAO, YIWEI ZHONG, LEI GUO, and ZHANCHENG GUO

In situ observation on the morphology evolution and phosphorous migration of gaseous-reduced, high-phosphorous oolitic iron ore during the melting process was carried out with a high-temperature confocal scanning laser microscope. The results showed that 1473 K (1200 °C) was a critical temperature at which the gangue minerals started to form into the slag phase while the iron grains remained in a solid state; in addition, the phosphorus remained in the slag phase. Since the separation of iron grains and P-bearing slag was not achieved at the low temperature under the conventional conditions, separate experiments of the iron phase and the P-bearing slag phase from gaseous-reduced, high-phosphorous oolitic iron ore at 1473 K (1200 °C) by super gravity were carried out in this study. Based on the iron-slag separation by super gravity, phosphorus was removed effectively from the iron phase at the temperature below the melting point of iron. Iron grains moved along the super-gravity direction, joined, and concentrated as the iron phase on the filter, whereas the slag phase containing apatite crystals broke through the barriers of the iron grains and went through the filter. Consequently, increasing the gravity coefficient was definitely beneficial for the separation of the P-bearing slag phase from the iron phase. With the gravity coefficient of $G = 1200$, the mass fractions of separated slag and iron phases were close to their respective theoretical values, and the mass fraction of MFe in the separated iron phase was up to 98.09 wt pct and that of P was decreased to 0.083 wt pct. The recovery of MFe in the iron phase and that of P in the slag phase were up to 99.19 and 95.83 pct, respectively.

DOI: 10.1007/s11663-015-0575-8

© The Minerals, Metals & Materials Society and ASM International 2016

I. INTRODUCTION

THE iron ore deposits exhibit an increasing complex mineralogical composition as the gradual decrease of high-grade iron ore resources around the world, so utilization of the refractory iron ore has been urgently needed. Simultaneously, there are multitudes of high-phosphorous iron ore resources in China with a reservation up to 2200 million ton,^[1] in which the mass fraction of phosphorus is 0.8 to 1.2 wt pct, and so it could not be supplied on a large scale for Blast Furnace iron making. Furthermore, the conventional beneficiation methods currently face great difficulties in removing the phosphorous phase from these iron ore due to its special oolitic structure and the intimate intermixing of apatite, hematite, and gangue minerals, such as the magnetic separation process and reverse flotation process.^[2-6] So far, many technical routes have been proposed across the world for the phosphorus removal and iron recovery from high-phosphorous iron ores,

including the acid leaching process,^[7-9] the alkaline leaching process,^[10,11] the bioleaching process,^[12-15] the combined hydrometallurgy process,^[16] and the coal-based and gas-based direct reduction processes.

As one of the typical direct reduction process for iron recovery from high-phosphorous iron ore, the coal-based reduction is always assisted with some physical methods to separate reduced iron and other gangue minerals from the sintering reduced ore, such as the fine grinding and magnetic separation process.^[17] According to thermodynamic data of the reactions between carbon and ore phases, an increasing temperature is beneficial for the improvement of the reduction rate, whereas the sintering degree of the reduced phase will also increase and restrict the following separation process. What is more, the apatite will be also reduced by carbon to Fe_2P , P_2 vapor or PO vapor successively as the temperature rises to 1129 K, 1471 K, or 1771 K (856 °C, 1198 °C, or 1498 °C), which can be further incorporated into the reduced iron. Conversely, lowering the temperature is beneficial for keeping the phosphorus out of reduced iron but hindering the reduction rate during the coal-based reduction process. To remove phosphorus from the reduced iron, Matinde,^[18,19] Yu,^[20] and Bai^[21] have investigated the function of dephosphorization by adding $\text{Ca}(\text{OH})_2$ or Na_2CO_3 to the coal-based reduction, and the experimental results have showed that the additives were beneficial for the dephosphorization from reduced iron.

JINTAO GAO and YIWEI ZHONG, Lecturers, LEI GUO, Doctoral Student, and ZHANCHENG GUO, Professor, are with the State Key Laboratory of Advanced Metallurgy, University of Science and Technology Beijing, Beijing 100083, P.R. China. Contact e-mail: zcguo@ustb.edu.cn

Manuscript submitted October 22, 2015.

Article published online January 22, 2016.

Compared with the coal-based direct reduction process, iron oxide in the ore can be reduced by reducing gas (H_2 or CO) at the temperature lower than 1273 K (1000 °C), whereas the apatite would not be reduced in this temperature range based on the thermodynamic data of the reactions between ore phases and H_2 or CO .^[20–22] Hence, Guo,^[22] Zhao,^[23,24] and Tang^[25] investigated the gas-based direct reduction of high phosphorous iron ore powders by H_2 or CO at the temperature of 1073 K to 1273 K (800 °C to 1000 °C) in the fluidized bed or in a tube furnace, the experimental results showed that iron oxide in the ore could be reduced by H_2 or CO at a lower temperature and reached a high reduction extent with the phosphorus still existing in apatite, whereas the reduction time in a fluidization state was faster than that of static reduction. To enhance the gas-based reduction, Omran^[26–29] studied the function of microwave heating on the structure of high-phosphorous oolitic iron ores and found that the oolitic unit generated cracks and fissures due to the microwave treatment, which could improve the phosphorus separation and magnetic properties. Tang^[30] further investigated the gas-based reduction of iron ore powders after microwave treatment and found that the microwave treatment had an intensification effect on gas-based reduction, which could further reduce the gas internal resistance and increase the chemical reaction rate. In addition, the authors of the current study grinded the ore to ultrafine 0.01 to 0.001 mm by using a jet mill and reduced in a rotary furnace at 973 K to 1173 K (700 °C to 900 °C) for 4.3 to 16.7 min, and the metallization ratio of reduced ore reached 83.91 to 97.32 pct. However, it ran into one problem that the phosphorous phase and iron phase were not effectively separated from the ultrafine reduced ore by magnetic separation.^[31]

Gas-based direct reduction carried out at a lower temperature is always combined with a high-temperature, melt-separation process to separate molten metal and slag phases, and a high temperature of 1823 K to 1873 K (1550 °C to 1600 °C) is needed to achieve the effective separation of two molten phases, but almost all of the phosphorus in reduced ore would be smelted into the metal phase at the high temperature. Guo^[22] adopted the melt separation of hydrogen-reduced, high-phosphorous iron ore powders at 1823 K (1550 °C) and realized the effective separation of molten metal and slag, but the phosphorous content in the metal phase was up to 1.22 wt pct, which means that all of the phosphorus in reduced ore has migrated into the metal. Tang^[30] adopted the melt separation of hydrogen-reduced ore powders after microwave treatment further by adding different doses of CaO and Na_2CO_3 powders as the dephosphorizing agent at 1823 K to 1873 K (1550 °C to 1600 °C), and the phosphorous content in the metal decreased to a minimum of 0.31 wt pct. So far, the contradiction of metal-slag separation and phosphorus removal from the metal phase becomes the major difficulty of the high-temperature, melt-separation process.

When there is no carbon in the reduced ore, the transform and transmission mechanisms of phosphorus during the melt-separation process have not been

completely clarified yet. Zhao^[23–25] considered that phosphorus existed as apatite inclusions in the metal, and Tang^[30] attributed the phosphorus partition between slag and metal based on the thermodynamic calculations of $CaO-MgO-MnO-FeO-Al_2O_3-P_2O_5-SiO_2-NaO$ by the coexistence theory of the slag structure.^[32–34] Guo^[22] also inferred that phosphorus was smelted into metal due to the reactions between Fe and P_2O_5 evidenced by the thermodynamic calculations. Fukagai and Tsukihashi^[35,36] studied the reaction mechanism of the $2CaO \cdot SiO_2$ and $FeO_x-CaO-SiO_2-P_2O_5$ slag, and they reported that the $CaO-SiO_2-P_2O_5$ solid phases with high P_2O_5 content and the $FeO-CaO-SiO_2$ system coexisted at 1573 K (1300 °C). Therefore, if the iron-slag separation temperature can be reduced below the melting point temperature of iron, it would be beneficial not only for keeping phosphorus out of the iron grains but also for the concentrating of phosphorus in the slag.

In this study, *in situ* observation on the morphology evolution and phosphorous migration of gaseous-reduced, high-phosphorous oolitic iron ore during the melting process were first carried out by a high-temperature confocal scanning laser microscope, to determine the critical temperature at which the slag phase starts to form while iron grains remain in a solid state. Nevertheless, it was impossible to accomplish the iron-slag separation at this low temperature under the conventional conditions. Inspired by the successful application of super-gravity technology in preparation of functionally gradient materials^[37,38] and removing inclusion from alloy melt,^[39,40] the experiments on separating the iron phase and the P-bearing slag phase from gaseous-reduced, high-phosphorous oolitic iron ore at 1473 K (1200 °C) by super gravity were carried out, and the feasibility of the process was verified in this study. Simultaneously, the effect of the super-gravity field on the microstructures, mineral compositions, components, and recovery ratio of MFe and P in the separated products was also investigated.

II. EXPERIMENTAL

A. Apparatus

1. High-temperature confocal scanning laser microscope

The *in situ* observation on the melting process of reduced iron ore was performed by the high-temperature confocal scanning laser microscope, which was composed of a confocal scanning laser microscope (Nikon VL2000DX) and a high-speed heating furnace (Yonekura SVF17SP) as illustrated in Figure 1.

2. Centrifugal apparatus

The super-gravity field used in the separation experiments of reduced iron ore was generated by the centrifugal apparatus as illustrated in Figure 2. The heating furnace was heated by the resistance wire with the isothermal zone 80 mm long, and the temperature was controlled by a program controller with an R-type thermocouple, which was within the observed precision

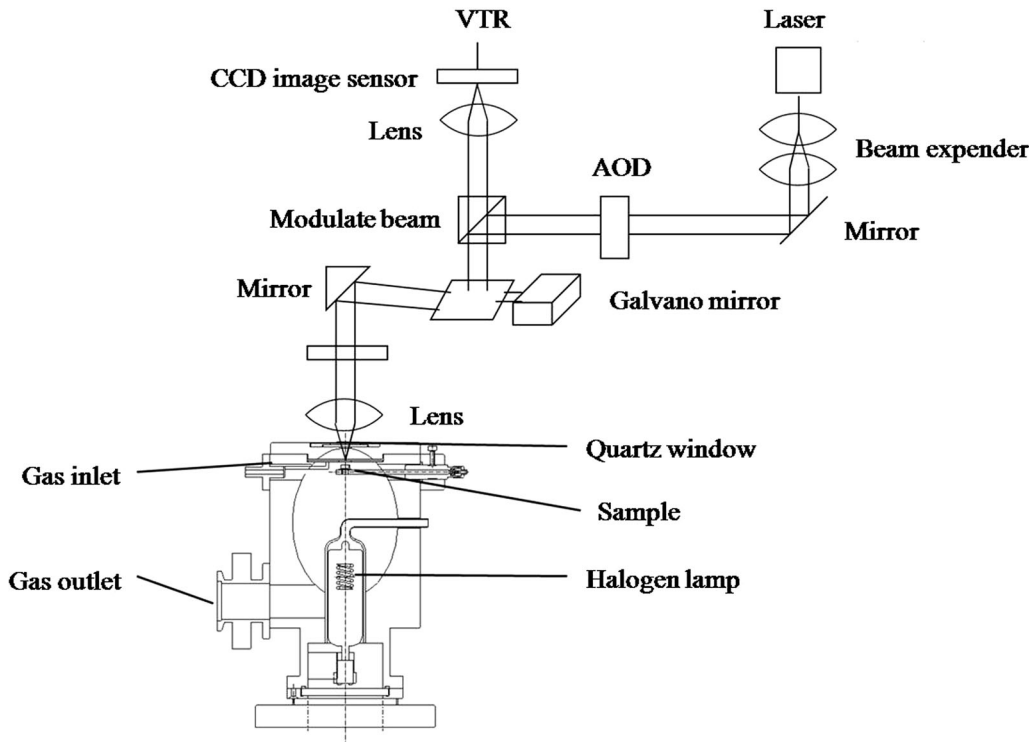


Fig. 1—Sketch of the high-temperature confocal scanning laser microscope.

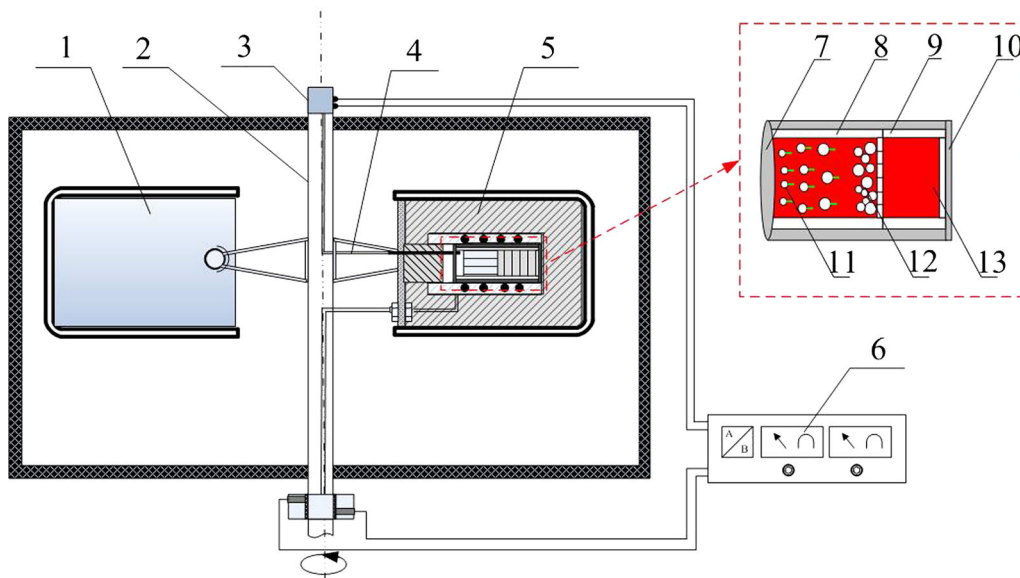


Fig. 2—Sketch of the centrifugal apparatus: 1 counterweight, 2 centrifugal axis, 3 conductive slipping, 4 thermocouple, 5 insulating layer, 6 temperature controller, 7 graphite lid, 8 alumina filter, 9 alumina crucible, 10 graphite crucible, 11 iron grains, 12 iron phase, 13 slag phase.

range of ± 3 K. The heating furnace and a counterweight were fixed symmetrically onto the centrifugal rotor. Once the centrifugal rotor started running, the heating furnace and counterweight change from vertical to horizontal and rotate therewith.

B. Material

The chemical compositions and mineralogical compositions of high-phosphorous iron ore from the Hubei

province of China are shown in Table I and Figure 3. The mass fraction of total iron (TFe) and phosphorus (P) are 50.15 wt pct (69.91 wt pct Fe_2O_3 and 1.68 wt pct Fe_3O_4) and 0.81 wt pct, respectively, and the mineral phases mainly includes hematite, quartz, and apatite. In this study, after crushed and screened to powders in the size of 0.11 to 0.90 mm, the ore powders were reduced in the fluidized bed with a gas flow of 2.0 L/minute H_2 and 1.0 L/minute Ar at 1073 K (800 °C) for 120 minutes. Then the samples obtained were used for the melting

Table I. Chemical Compositions (Weight Percent) of the High-Phosphorous Oolitic Iron Ore

Composition	TFe	Fe ₂ O ₃	Fe ₃ O ₄	SiO ₂	CaO	Al ₂ O ₃	MgO	P
Content	50.15	69.91	1.68	13.15	4.80	4.52	0.48	0.81

Table II. Chemical Compositions (Weight Percent) of the Gaseous-Reduced, High-Phosphorous Oolitic Iron Ore

Composition	TFe	FeO	MFe	SiO ₂	CaO	Al ₂ O ₃	MgO	P
Basicity of 0.37	64.44	16.58	51.55	16.89	6.17	5.81	0.62	1.04
Basicity of 1.0	58.20	14.97	46.55	15.25	15.25	5.25	0.56	0.94

experiments in normal gravity and the separation experiments in super gravity. Simultaneously, the ore particles in the size of 3.0 to 5.0 mm were reduced in a tube furnace with a gas flow of 0.5 L/minute H₂ at 1073 K (800 °C) for 210 min to obtain the same average metallization ratio, and then the samples were used for an *in situ* observation experiment by high-temperature CSLM. With the help of X-ray diffraction (XRD) and scanning electron microscope-energy-dispersive spectrum (SEM-EDS) analysis, the variations of the mineralogical composition and microstructure of the ore powders before and after gaseous reduction are shown in Figures 3 and 4. Obviously, the hematite coexisting with the quartz builds the concentric shell of oolites (0.2 to 0.5 mm) in the raw ore, and the fine apatite heterogeneously distributes in the oolitic layers. After gaseous reduction, only the hematite was reduced into metallic iron, while the phosphorus remained in the form of apatite. Hence, it provides the possibility for the following separation of the iron and P-bearing slag from the reduced ore.

C. Experimental Procedure

1. *In situ* observation on the melting process by high-temperature CSLM

To investigate the morphology evolution with the increasing temperature, the *in situ* observation on the melting process of reduced ore was first carried out by high-temperature CSLM. The reduced ore particles with the size of 3.0 to 5.0 mm were cut into slices with a height of 1.0 to 2.0 mm and polished. One was put into an aluminum crucible with an inner diameter of 5.0 mm, and then the crucible was placed in the center of the furnace under the confocal scanning laser microscope; the lens of the microscope was aimed at one oolite of the sample with a magnification of $\times 1100$. After that, the air was flushed out from the furnace by pulling a vacuum on it, and the sample was rapidly heated in argon atmosphere from room temperature to 1173 K (900 °C) at a heating rate of 200 K/minute (°C/minute) and then heated to 1673 K (1400 °C) at a heating rate of 100 K/minute (°C/minute); then it was further heated to 1773 K (1500 °C) at a heating rate of 50 K/minute (°C/minute). Finally, the sample was cooled at a cooling rate of 200 K/minute (°C/minute). Meanwhile, the images captured during the melting process were recorded on the DVD at a rate of 1 frame/second for analyzing the morphology evolution at different temperatures.

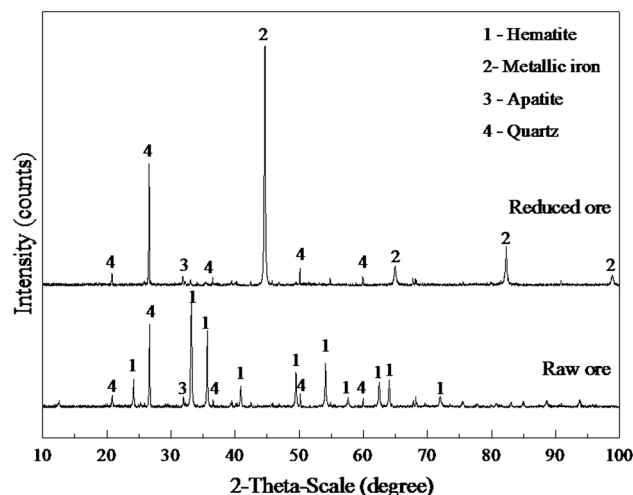


Fig. 3—XRD patterns of the high-phosphorous oolitic iron ore before and after gaseous reduction.

2. Melting experiments in normal gravity field

To investigate the phosphorus migration between slag and iron phases at different temperatures, the melting experiments of reduced ore were further carried out at 1373 K to 1673 K (1100 °C to 1400 °C). An amount of 10 g of the reduced ore powders with a size of 0.11 to 0.90 mm were put into an alumina crucible with an inner diameter of 12 mm, which was further put into a graphite crucible with an inner diameter of 19 mm and covered with a graphite lid to avoid the reoxidation of reduced iron. And then the samples were heated to the fixed temperatures of 1473 K, 1573 K, or 1673 K (1200 °C, 1300 °C, or 1400 °C), respectively. After melting at the constant temperature for 10 minutes, the graphite crucible was taken out and water-quenched.

3. Iron-slag separation experiments in a super-gravity field

Based on the earlier melting experiments, the separation experiments of reduced ore powders at 1473 K (1200 °C) were carried out in a super-gravity field. The slag basicity defined as CaO/SiO₂ was adjusted from 0.37 to 1.0 by adding CaO into the reduced ore to obtain a lower melting temperature of the slag phase based on the CaO-SiO₂-FeO phase diagram and the experimental results of Guo,^[22] Tang,^[30] and Tsukihashi^[35,36] as shown in Table II. An amount of 10 g of reduced ore powders were put into an alumina filter (I.D. 12 mm) with the pore

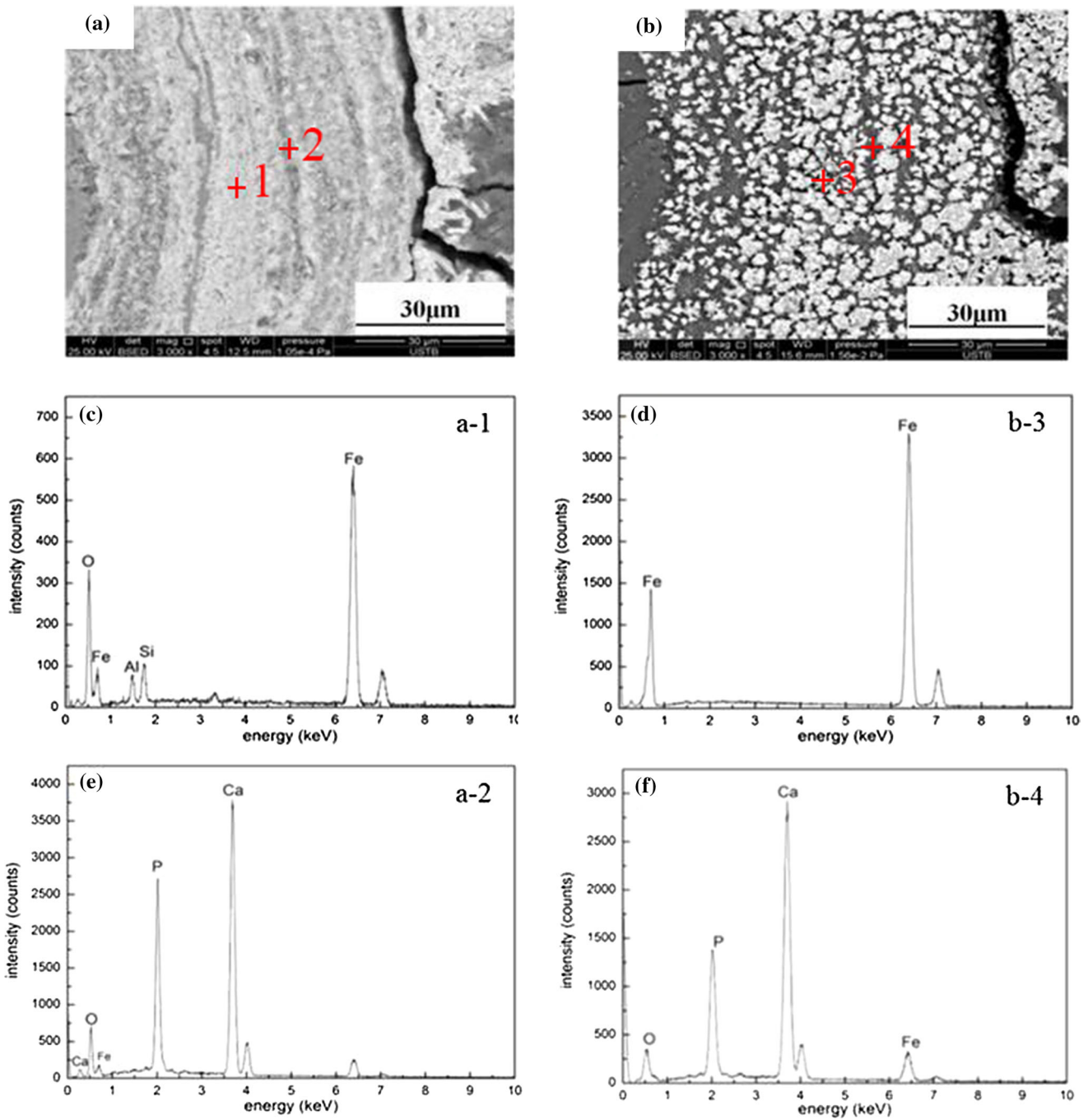


Fig. 4—SEM-EDS photographs of the high-phosphorous oolitic iron ore before and after gaseous reduction: (a) and (b) SEM of raw ore and reduced ore, (c) and (d) EDS of hematite before and after reduction, and (e) and (f) EDS of apatite before and after reduction.

size of $d = 0.5$ mm and then put into an alumina crucible with an inner diameter of 14 mm, which were further put into a graphite crucible with an inner diameter of 19 mm and covered with a graphite lid and heated to 1473 K (1200 °C) in the heating furnace of a centrifugal apparatus; then the centrifugal apparatus was started and adjusted to the specified angular velocity of 1036 RPM,

1465 RPM, 1794 RPM, or 2072 RPM; namely, $G = 300$, 600, 900, or 1200 at the constant 1473 K (1200 °C) for 10 minutes, respectively. After that, the centrifugal apparatus was shut off, and the graphite crucible was taken out and water-quenched. Simultaneously, the parallel experiment was carried out at 1473 K (1200 °C) for 10 minutes in normal gravity ($G = 1$).

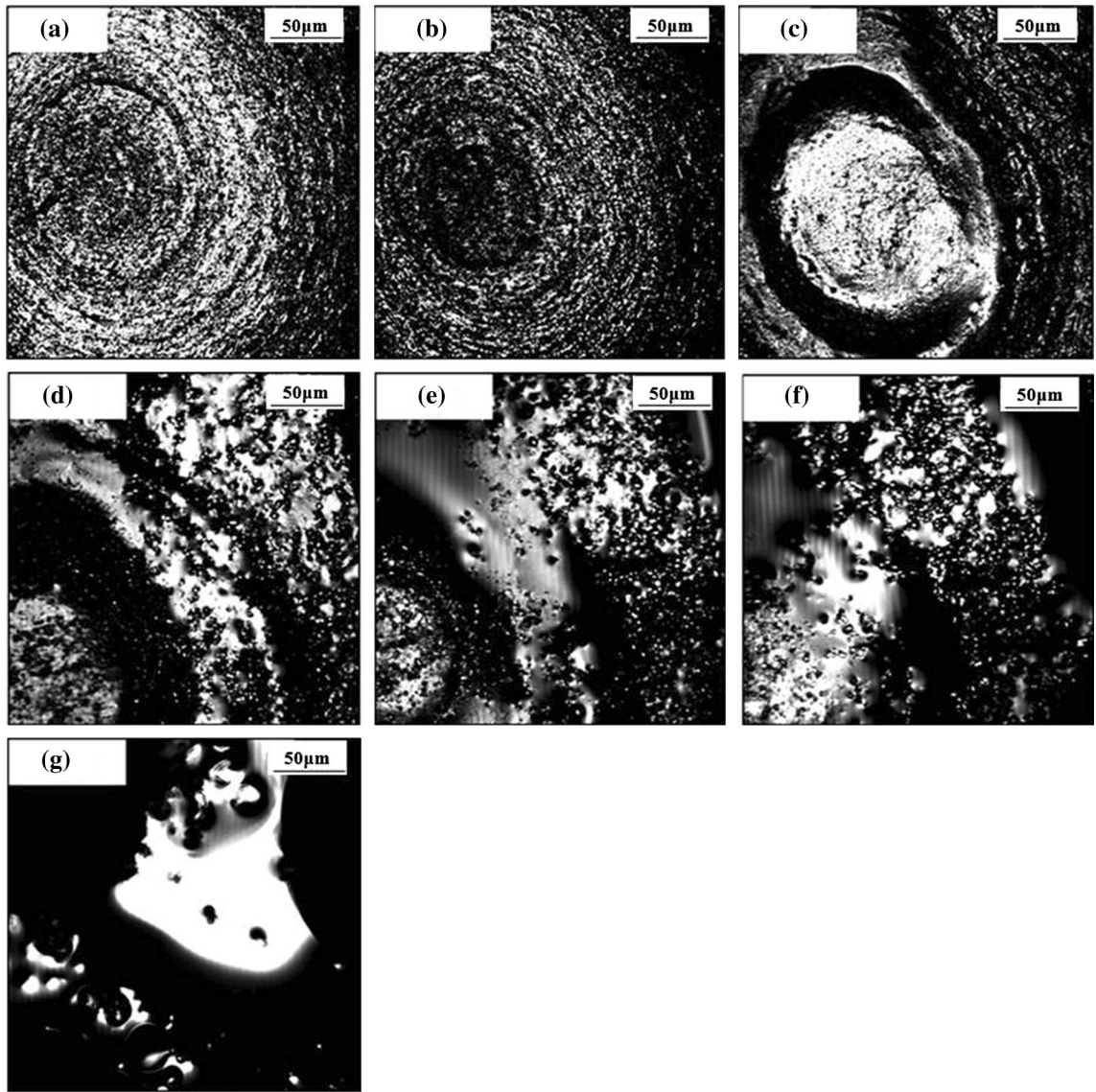


Fig. 5—*In situ* observation on morphology evolution of the sample surface in different temperatures by high-temperature CSLM: (a) 1173 K (900 °C), (b) 1273 K (1000 °C), (c) 1373 K (1100 °C), (d) 1473 K (1200 °C), (e) 1573 K (1300 °C), (f) 1673 K (1400 °C), and (g) 1773 K (1500 °C).

D. Analysis and Characterization

The average metallization ratio is defined as the ratio of the metallic iron component to the total iron component *via* Eq. [1]:

$$M_R = \frac{M_{\text{Fe}}}{T_{\text{Fe}}} \times 100 \text{ pct} \quad [1]$$

where M_R is the average metallization ratio (pct), M_{Fe} is the mass fraction of metallic iron (wt pct), and T_{Fe} is the mass fraction of total iron (wt pct).

The gravity coefficient is defined as the ratio of super-gravitational acceleration to normal-gravitational acceleration *via* Eq. [2]:

$$G = \frac{\sqrt{g^2 + (\omega^2 R)^2}}{g} = \frac{\sqrt{g^2 + \left(\frac{N^2 \pi^2 R}{900}\right)^2}}{g} \quad [2]$$

where G is the gravity coefficient, g is the normal-gravitational acceleration ($g = 9.80 \text{ m/s}^2$), ω is the angular velocity ($\text{rad} \times \text{s}^{-1}$), N is the rotating speed of the centrifugal (RPM), and R is the distance from the centrifugal axis to the center of the sample ($R = 0.25 \text{ m}$).

The recovery ratio of MFe is defined as the ratio of the metallic iron weight in a separated iron phase to the total metallic iron weight in both iron and slag phases *via* Eq., [3] and the recovery ratio of P is defined as the ratio of the phosphorus weight in a separated slag phase to the total phosphorus weight *via* Eq. [4]:

$$\varepsilon_{\text{MFe}} = \frac{m_{\text{I}} \times \omega_{\text{MFe-I}}}{m_{\text{I}} \times \omega_{\text{MFe-I}} + m_{\text{S}} \times \omega_{\text{MFe-S}}} \times 100 \text{ pct} \quad [3]$$

$$\varepsilon_{\text{P}} = \frac{m_{\text{S}} \times \omega_{\text{P-S}}}{m_{\text{S}} \times \omega_{\text{P-S}} + m_{\text{I}} \times \omega_{\text{P-I}}} \times 100 \text{ pct} \quad [4]$$

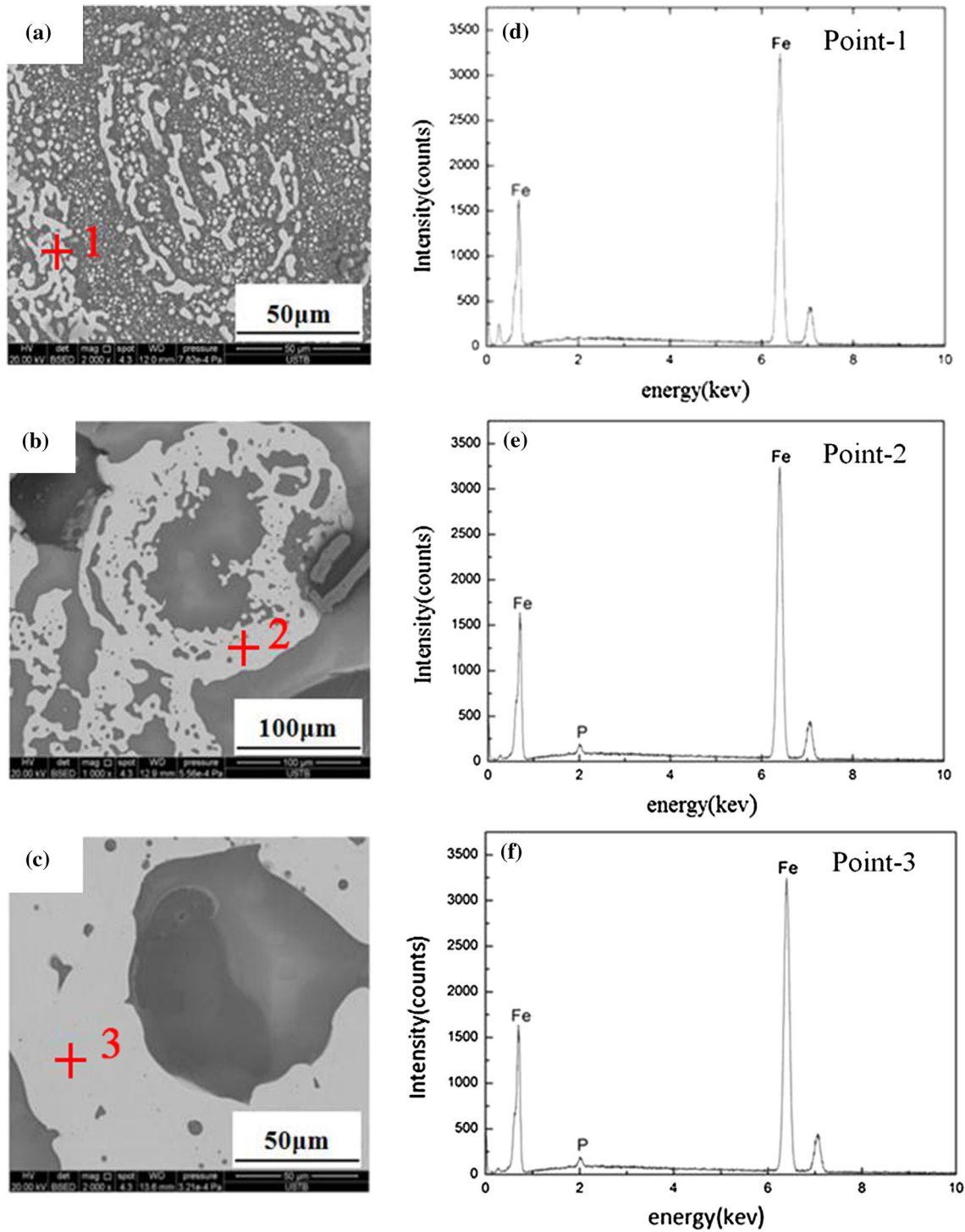


Fig. 6—SEM-EDS photographs of the samples after melting at different temperatures: (a)–(c) SEM of the samples melted at 1473 K (1200 °C), 1573 K (1300 °C), and 1673 K (1400 °C); and (d) through (f) EDS of iron phase in the samples melted at 1473 K (1200 °C), 1573 K (1300 °C), and 1673 K (1400 °C).

where ε_{MFe} and ε_P are the recovery ratio of MFe in the separated iron phase and that of P in the separated slag phase, m_I and m_S are the mass fractions of the separated iron phase and slag phase, w_{MFe-I} and w_{MFe-S} are the mass fractions of metallic iron in the

separated iron phase and slag phase, and w_{P-S} and w_{P-I} are the mass fractions of phosphorus in the separated slag phase and iron phase.

The samples obtained by melting at different temperatures in normal gravity were sectioned longitudinally

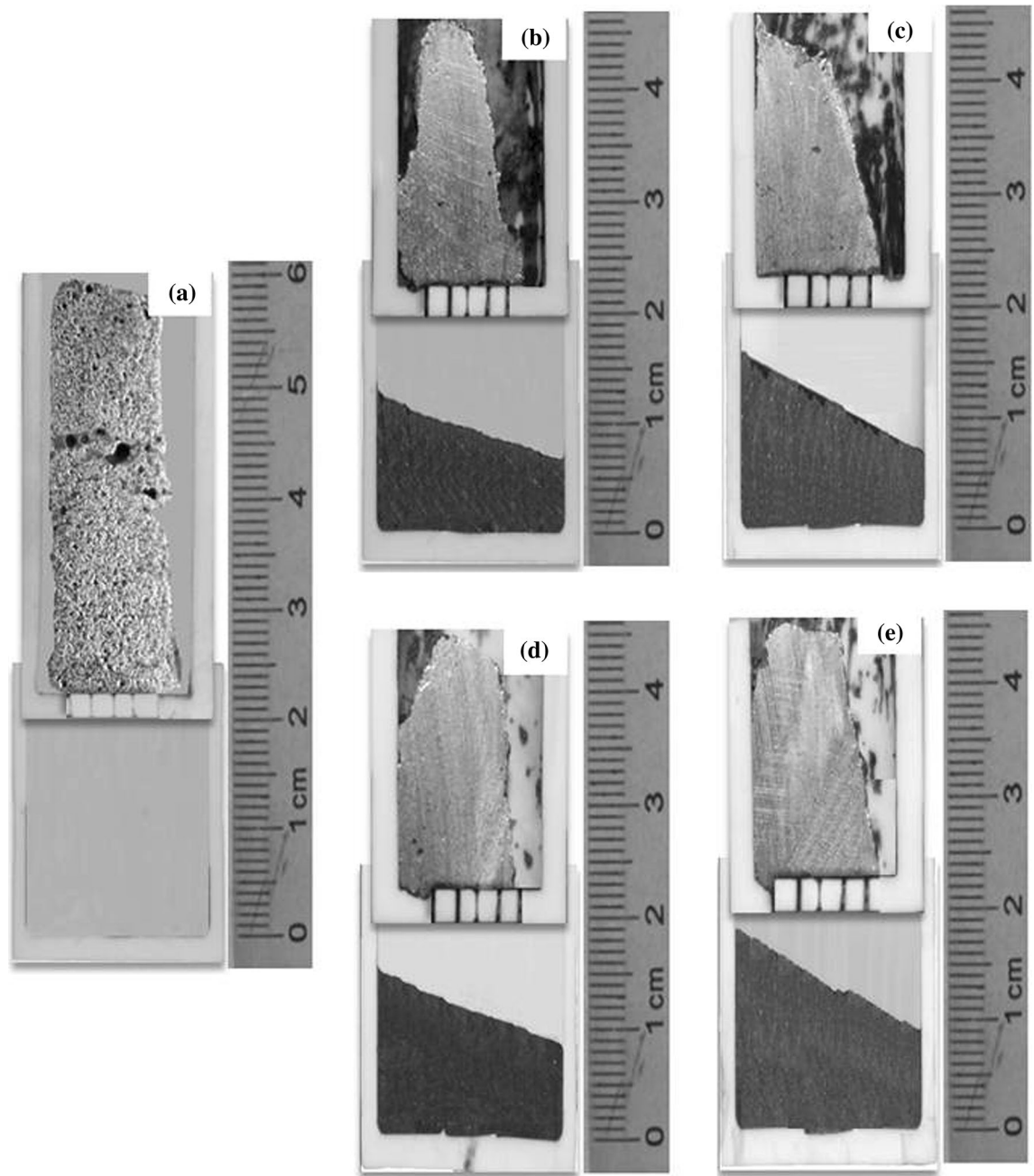


Fig. 7—Vertical sections of the samples obtained by super-gravity separation compared with the sample in normal gravity: (a) $G = 1$, (b) $G = 300$, (c) $G = 600$, (d) $G = 900$, and (e) $G = 1200$.

along the center axis and then measured on the scanning electron micrograph and energy-dispersive spectrum to gain the microstructures and mineral compositions of samples after melting at different temperatures.

As for the samples obtained by super-gravity separation at 1473 K (1200 °C), the samples that held on and went through the filter were also sectioned longitudinally along the direction of super gravity. And then the sample was measured by the scanning electron micrograph and energy-dispersive spectrum for analyzing the respective microstructures and mineral composi-

tions of the iron and slag phases, as well as the distribution and mineral composition of the phosphorous phase in different areas of the sample. Simultaneously, the iron phase and slag phase were crossly divided along the filter and measured respective weights, and then further measured by the chemical analytical method and the ICP method with OPTIMA 7000DV to determine the respective mass fractions of metallic iron (MFe) and phosphorus (P). Then the recovery ratio of MFe in iron phase and that of P in slag phase were calculated.

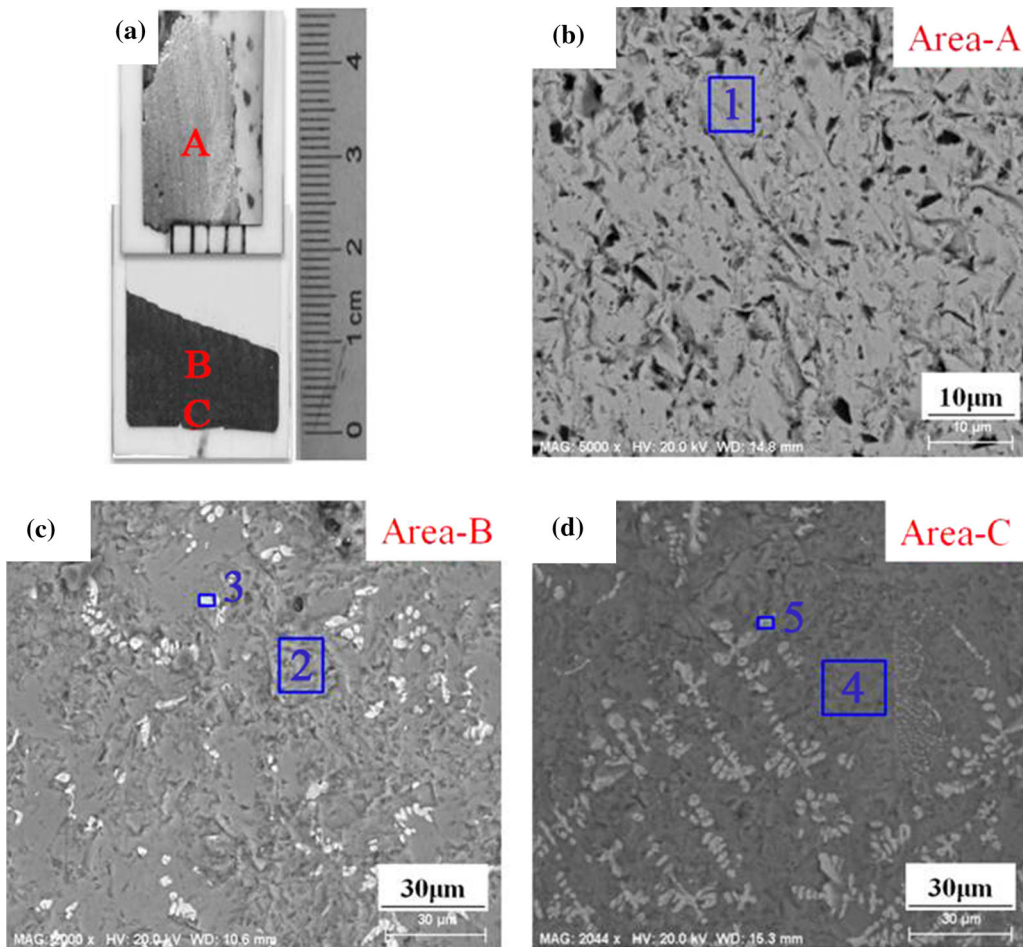


Fig. 8—SEM photographs of different areas in the sample obtained by super-gravity separation with $G = 900$: (a) positions of different areas in the sample, (b) SEM of iron phase, (c) SEM in the upper area of the slag phase, and (d) SEM in the bottom area of the slag phase.

III. RESULTS AND DISCUSSION

A. *In Situ* Observation on Morphology Evolution at Different Temperatures by High-Temperature CSLM

The *in situ* observation results on the morphology evolution of the sample surface from 1173 K to 1773 K (900 °C to 1500 °C) by high-temperature CSLM are shown in Figure 5. Since confocal scanning laser microscope displays the true color of different mineral phases in the sample, the light-colored areas represent the iron phase and the dark-colored areas represent the gangue phase. Obviously, some of the gangue phases started to slightly soften in the temperature range of 1173 K to 1373 K (900 °C to 1100 °C), which led to the converging of fine iron layers and the scattering of inner oolitic layers. And the changes of mineral structure only occurred among the layers within the oolitic and it did not break through the outer boundary of the oolitic. When the temperature was up to 1473 K (1200 °C), the gangue minerals started to form into the slag phase, and the slag phase started to move and break through the oolitic outer boundary. As a result, the view field moved a little toward the outer border but remained in the same oolitic. With the temperature further increased from

1473 K to 1673 K (1200 °C to 1400 °C), the diffusion coefficient increased from a microscopic view, whereas the viscosity of slag decreased from a macroscopic view, and thus, the fluidity of slag was improved. The slag within one oolitic gathered into the slag phase with that of adjacent oolitics, and the iron grains also gathered together. But the aggregation process was relatively slow in this temperature range. When it came to about 1773 K (1500 °C), the liquidity of the sample became better, and the iron also formed into the liquid phase and covered with the floating slag.

B. Phosphorous Migration After Melting at Different Temperatures

To investigate further the phosphorus migration between slag and iron phases after melting at different temperatures, the SEM-EDS analysis on the samples obtained by melting at 1473 K to 1673 K (1200 °C to 1400 °C) was carried out, with the results shown in Figure 6. As for the sample after melting at 1473 K (1200 °C), the minerals maintained in the oolitic structure with the inner layer scattered and the outer border broke as the gangue minerals started to form into the

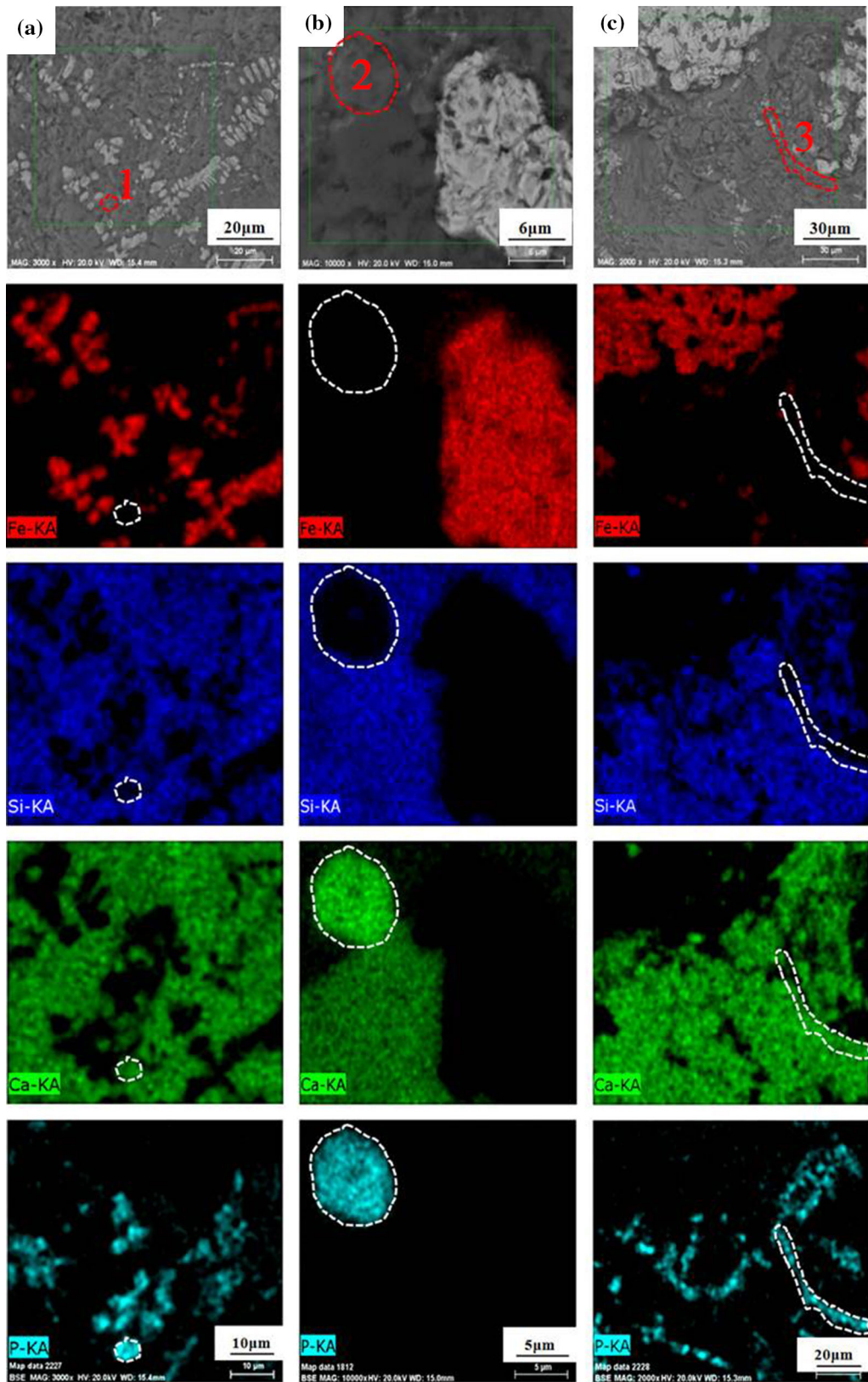


Fig. 9—SEM-EDS mapping of phosphorous-rich phases in different areas of the sample obtained by super-gravity separation with $G = 900$: (a) in the bottom area of the slag phase, (b) larger version of the phosphorous phase, and (c) in residual slag in the filtering holes.

slag phase and move, but the phosphorus still existed in the slag phase rather than in the iron phase. After melting at 1573 K (1300 °C), the inner layers of oolite disappeared, and the outer boundary was no longer clear as the fluidity of slag was improved. The iron grains started to slightly soften, but some phosphorus started to immigrate into the iron phase. When the melting temperature further increased up to 1673 K (1400 °C), the oolitic structure was destroyed with the iron and slag gathered into two phases, and more phosphorus smelted into the iron phase. This indicated that the 1473 K (1200 °C) was a critical temperature at which the gangue minerals started to form into the slag phase, which occurs because the compositions of the main minerals (SiO_2 , CaO , FeO , and Al_2O_3) were in the liquid area lower than 1573 K (1300 °C) based on the (CaO - SiO_2 - FeO - Al_2O_3) phase diagram reported by Phillips^[41] and Tsukihashi.^[42,43] Meanwhile, the iron grains remained in a solid state, whereas the phosphorus

sustained in the slag phase. However, it was impossible to achieve the separation of iron grains and P-bearing slag at the low temperature under the conventional conditions.

C. Separation of Iron and P-bearing Slag Phases at 1473 K (1200 °C) by Super Gravity

1. Macro and micro structures of the samples obtained by super-gravity separation

The vertical sections of the samples obtained by super-gravity separation with the gravity coefficient of $G = 300, 600, 900$, and 1200 compared with the gravity coefficient of $G = 1$ are illustrated in Figure 7. In a macroscopic view, the layered structures appeared significantly in the samples obtained by super-gravity separation. The sample that held on the filter appeared as a bright white, compact structure, and the sample that went through the filter presented in a black, glassy state. However, the whole sample that was held on the filter remained in normal gravity field, and a uniform structure was presented in the sample.

Combined with the SEM-EDS analysis, the microstructures and mineral compositions of the separated samples obtained by super-gravity separation with $G = 900$ are shown in Figure 8 and Table III, respectively. Obviously, the sample that held on the filter was in the iron phase, and the sample that went through the filter was in the slag phase. In a microscopic view, the separated iron phase exhibited the porous structure including some fine pores (Figure 8(b)). And the separated slag phase appeared as a compact structure with some fine dendritic crystals of iron distributed in the bottom area (Figure 8(c)) and some in the upper areas (Figure 8(d)). It was evident that the iron grains moved directionally along the direction of super gravity, joined, and concentrated as the iron phase on the filter. In contrast, the slag phase broke through the barriers of iron grains and went through the filter, and then concentrated in the bottom alumina crucible.

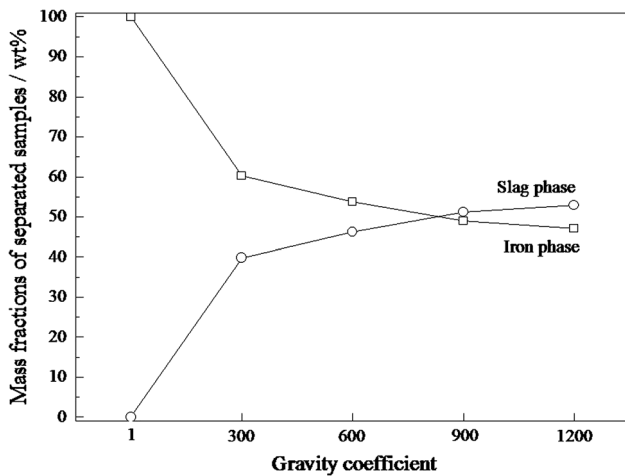


Fig. 10—Mass fractions of separated samples obtained by super-gravity separation with different gravity coefficients.

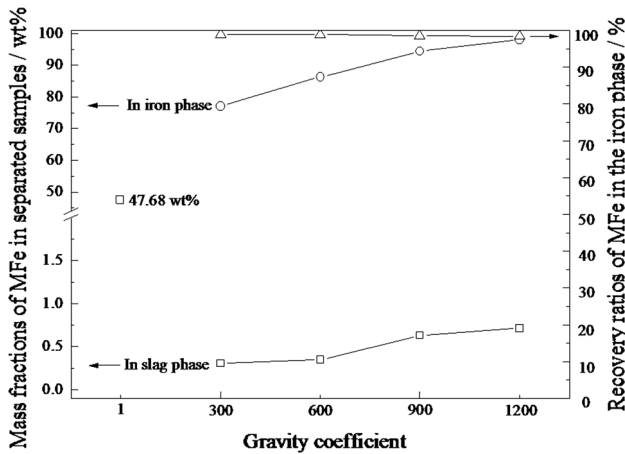


Fig. 11—Mass fractions and recovery ratios of MFe in the separated samples obtained by super-gravity separation with different gravity coefficients.

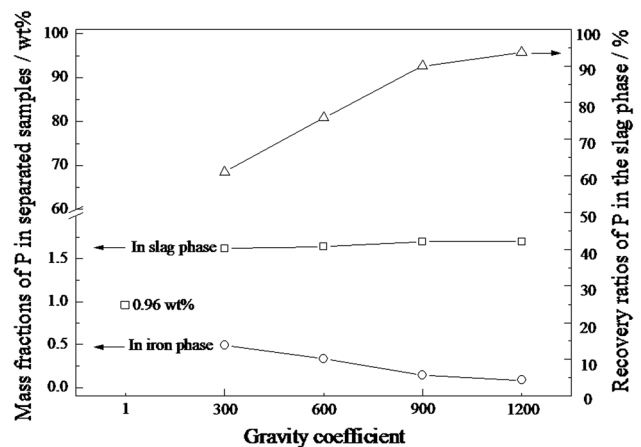


Fig. 12—Mass fractions and recovery ratios of P in the separated samples obtained by super-gravity separation with different gravity coefficients.

Table III. Energy-Dispersive Spectrum Data (Wt Pct) of Different Areas in the Sample Obtained by Super-Gravity Separation with $G = 900$

Position	Area	Fe	Ca	Si	Al	Mg	O	P
Iron phase	Fig. 8(b):1	99.49	0.08	0.11	—	—	0.32	—
In the upper area of slag phase	Fig. 8(c):2	21.53	22.17	13.95	3.76	0.34	38.24	0.01
	Fig. 8(c):3	99.49	—	—	—	—	0.51	—
In the bottom area of slag phase	Fig. 8(d):4	23.10	20.19	12.94	5.11	0.64	36.08	1.94
	Fig. 8(d):5	99.27	—	0.14	—	—	0.59	—

Table IV. Energy-Dispersive Spectrum Data (Wt Pct) of Phosphorous-Rich Phases in Different Areas of the Sample Obtained by Super-Gravity Separation with $G = 900$

Position	Area	P	Ca	O	Si
In the bottom area of the slag phase	Fig. 9(a):1	19.27	37.42	41.07	2.24
Larger version of the phosphorous phase	Fig. 9(b):2	19.96	40.15	39.06	0.83
In residual slag in the filtering holes	Fig. 9(c):3	19.13	39.38	39.72	1.77

2. Distribution and mineral composition of phosphorous phase in the separated samples

To investigate further the distribution and mineral composition of the phosphorous phase, the SEM–EDS mapping in different areas of the separated samples obtained by super-gravity separation was carried out. As shown in Figure 9(a), the phosphorous phases mainly concentrated in the bottom area of the slag phase, and these phosphorous-rich phases were in the form of equiaxed crystals with a size less than 0.02 mm and concentrated as some clusters. Combined with the corresponding energy-dispersive spectrum data in Table IV, the phosphorous-rich phases mainly comprised phosphorus (19.13 to 41.07 wt pct), and a small amount of silicon (0.83 to 2.24 wt pct). It was indicated that the phosphorus still existed in the form of the apatite phase, which can be confirmed intuitively by the SEM–EDS mapping on the larger version of the phosphorous concentrated phase as shown in Figure 9(b). The fine apatite crystals moved out of the oolites with the slag phase along the direction of super gravity and went through the filter, and then they concentrated in the bottom area of the slag phase due to the density difference with the slag phase. Furthermore, the apatite crystals in residual slag in the filtering holes presented an obvious movement track along the super-gravity direction as shown in Figure 9(c), further indicating the directional migration of apatite crystals in the super-gravity field.

3. Components and recovery ratios of MFe and P in the separated samples

Figure 10 presents the mass fractions of separated slag and iron phases obtained by super-gravity separation with different gravity coefficients. Due to the density difference between iron grains and the slag phase, the super-gravity field could definitely increase the diffusion coefficient of slag and force it to move directionally and then separate from iron grains. Therefore, increasing the gravity coefficient could effectively increase its separation effect. Consequently, with the gravity coefficient of $G = 1200$, the mass fraction of the

separated slag phase and iron phase were up to 52.93 and 47.07 wt pct, respectively, which were close to their respective theoretical values.

Measured by the chemical analytical method, the mass fractions of MFe in the separated iron and slag phases obtained by super-gravity separation with different gravity coefficients are shown in Figure 11. Compared with the mass fraction of MFe at the gravity coefficient of $G = 1$ (47.68 wt pct), increasing the gravity coefficient from $G = 300$ to 1200 can enhance the mass fraction of MFe in the iron phase from 77.08 wt pct to 98.09 wt pct, whereas that in the slag phase was only 0.31 to 0.71 wt pct. The recovery ratio of MFe in the separated iron phase was up to 99.74 to 99.19 pct. Simultaneously, the mass fractions of P in the separated iron and slag phases were measured by the ICP method as shown in Figure 12. Since the separation temperature was lower than the melting point of iron and not high enough for the active iron-slag interface reactions,^[22,30] the super-gravity field could effectively prevent the migration of phosphorus into the iron phase while it concentrated in the slag phase. Consequently, with the increase of the gravity coefficient from $G = 300$ to 1200, the mass fraction of P in the iron phase was decreased from 0.491 to 0.083 wt pct, and that in the slag phase was up to 1.620 to 1.702 wt pct. The recovery ratio of P in the separated slag phase was up to 68.55 to 95.83 pct.

IV. CONCLUSIONS

Based on the *in situ* observation results on the morphology evolution and phosphorous migration of gaseous-reduced, high-phosphorous oolitic iron ore during the melting process by high-temperature CSLM, the 1473 K (1200 °C) was a critical temperature at which the gangue minerals started to form into the slag phase while the iron grains remained in a solid state; in addition, the phosphorus remained in the slag phase.

The results confirmed that separating the iron phase and the P-bearing slag phase from gaseous-reduced, high-phosphorous oolitic iron ore by super gravity at

1473 K (1200 °C) was a feasible and effective method. The iron grains moved along the super-gravity direction, joined, and concentrated as the iron phase on the filter, while the slag phase containing apatite crystals broke through the barriers of the iron grains and went through the filter. Consequently, increasing the gravity coefficient was definitely beneficial for the separation of the P-bearing slag phase from the iron phase. With the gravity coefficient of $G = 1200$, the mass fractions of separated slag and iron phases were close to their respective theoretical values. The mass fraction of MFe in the separated iron phase was up to 98.09 wt pct and that of P was decreased to 0.083 wt pct. The recovery of MFe in the iron phase and that of P in the slag phase were up to 99.19 and 95.83 pct, respectively.

ACKNOWLEDGMENTS

This study is supported by the National Natural Science Foundations of China (Nos. 51404025 and 51234001) and the Fundamental Research Funds for the Central Universities (FRF-TP-15-009A2).

REFERENCES

- J. Wu, Z. Wen, and M. Chen: *Steel Res. Int.*, 2011, vol. 82, pp. 494–500.
- R.C. Guimaraes, A.C. Araugo, and A.E.C. Peres: *Miner. Eng.*, 2005, vol. 18, pp. 199–204.
- C.Y. Cheng, V.N. Misra, J. Clough, and R. Mun: *Miner. Eng.*, 1999, vol. 12, pp. 1083–92.
- S. Song, E.F. Campos-Toro, Y. Zhang, and A. Lopez-valdivieso: *Int. J. Miner. Metall. Mater.*, 2013, vol. 20, pp. 113–19.
- A.P.L. Nunes, C.L.L. Pinto, G.E.S. Valadao, and P.R.M. Viana: *Miner. Eng.*, 2012, vol. 39, pp. 206–12.
- X.Y. Hao, H.X. Dai, and Z.Q. Zhao: *Met. Miner.*, 2007, vol. 1, pp. 7–12.
- J.T. Yu, Z.C. Guo, and H.Q. Tang: *ISIJ Int.*, 2013, vol. 53, pp. 2056–64.
- Y. Zhang and M. Muhammed: *Hydrometallurgy*, 1989, vol. 21, pp. 255–275.
- M.J. Fisher-White, R.R. Lovel, and G.J. Sparrow: *ISIJ Int.*, 2012, vol. 52, pp. 1794–800.
- M.J. Fisher-White, R.R. Lovel, and G.J. Sparrow: *ISIJ Int.*, 2012, vol. 52, pp. 797–803.
- Y.S. Jin, T. Jiang, Y.B. Yang, L. Qian, L.G. Hui, and G.Y. Feng: *J. Cent. South Univ. Technol.*, 2006, vol. 13, pp. 673–77.
- O. Priha, T. Sarlin, P. Blomberg, L. Wendling, J. Makinen, M. Arnold, and P. Kinnunen: *Hydrometallurgy*, 2014, vol. 150, pp. 269–75.
- P. Delvasto, A. Valverde, A. Ballester, J.A. Munoz, F. Gonzalez, M.L. Blazquez, JM Igual, and C. Garcia-Balboa: *Hydrometallurgy*, 2008, vol. 92, pp. 124–29.
- P. Delvasto, A. Ballester, J.A. Munoz, F. Gonzalez, M.L. Blazquez, J.M. Igual, and C.G. Balboa: *Miner. Eng.*, 2009, vol. 22, pp. 1–9.
- T.M. Bhatti and W. Yawar: *Hydrometallurgy*, 2010, vol. 103, pp. 54–59.
- K. Ionkov, S. Grydardzhiev, A.C. de Araujo, D. Bastin, and M. Lacoste: *Miner. Eng.*, 2013, vols. 46–47, pp. 119–27.
- C.Y. Xu, T.C. Sun, J. Kou, Y.L. Li, X.L. Mo, and L.G. Tang: *Trans. Nonferrous Met. Soc. China*, 2012, vol. 22, pp. 2806–12.
- E. Matinde and M. Hino: *ISIJ Int.*, 2011, vol. 51, pp. 544–51.
- E. Matinde and M. Hino: *ISIJ Int.*, 2011, vol. 51, pp. 220–27.
- W. Yu, T.C. Sun, J. Kou, Y.X. Wei, C.Y. Xu, and Z.Z. Liu: *ISIJ Int.*, 2013, vol. 53, pp. 427–33.
- S.J. Bai, S.M. Wen, D.W. Liu, W.D. Zhang, and Y.J. Xian: *ISIJ Int.*, 2011, vol. 51, pp. 1601–07.
- L. Guo, J.T. Gao, Y.W. Zhong, H. Gao, and Z.C. Guo: *ISIJ Int.*, 2015, vol. 55, pp. 1806–15.
- Z.L. Zhao, H.Q. Tang, and Z.C. Guo: *J. Univ. Sci. Technol. Beijing*, 2009, vol. 31, pp. 964–69.
- Z.L. Zhao, H.Q. Tang, and Z.C. Guo: *J. Iron Steel Res.*, 2013, vol. 20, pp. 16–24.
- H.Q. Tang, Z.C. Guo, and Z.L. Zhao: *J. Iron Steel Res.*, 2010, vol. 17, pp. 1–6.
- M. Omran, T. Fabritius, and R. Mattila: *Powder Technol.*, 2015, vol. 269, pp. 7–14.
- M. Omran, T. Fabritius, N. Abdel-Khalek, and A. Elmahdy: *Appl. Surf. Sci.*, 2015, vol. 345, pp. 127–40.
- M. Omran, T. Fabritius, N. Abdel-Khalek, and A. Elmahdy: *Sep. Purif. Technol.*, 2014, vol. 136, pp. 223–32.
- M. Omran, T. Fabritius, N. Abdel-Khalek, M. El-Aref, A.E.-H. Elmaniwi, M. Nasr, and A. Elmahdy: *J. Miner. Mater. Charact. Eng.*, 2014, vol. 2, pp. 414–27.
- H.Q. Tang, D.W. Liu, H.Y. Zhang, and Z.C. Guo: *Metall. Mater. Trans. B*, 2014, vol. 45B, pp. 1683–94.
- J.T. Gao, L. Guo, and Z.C. Guo: *Metall. Mater. Trans. B*, 2015, vol. 46B, pp. 2180–89.
- J. Zhang: *Computational Thermodynamics of Metallurgical Melts and Solutions*. Metallurgical Industry Press, Beijing, China, 2007.
- X. Yang, J. Duan, C. Shi, M. Zhang, and Y. Zhang: *J. Wang. Metall. Mater. Trans. B*, 2011, vol. 42B, pp. 738–70.
- X. Yang, C. Shi, M. Zhang, J. Duan, and J. Zhang: *Metall. Mater. Trans. B*, 2011, vol. 42B, pp. 951–76.
- S. Fukagai, T. Hamano, and F. Tsukihashi: *ISIJ Int.*, 2007, vol. 47, pp. 187–89.
- T. Hamano, S. Fukagai, and F. Tsukihashi: *ISIJ Int.*, 2006, vol. 46, pp. 490–92.
- T.P.D. Rajan, R.M. Pillai, and B.C. Pai: *Int. J. Cast Metal Res.*, 2008, vol. 21, pp. 214–18.
- M.R. Rahimpour and M. Sobhani: *Metall. Mater. Trans. B*, 2013, vol. 44B, pp. 1120–23.
- L.X. Zhao, Z.C. Guo, Z. Wang, and M.Y. Wang: *Metall. Mater. Trans. B*, 2010, vol. 41, pp. 505–08.
- L.X. Zhao, Z.C. Guo, Z. Wang, and M.Y. Wang: *Metall. Mater. Trans. A*, 2010, vol. 41A, pp. 670–75.
- B. Phillips and A. Muan: *J. Am. Ceram. Soc.*, 1959, vol. 42, pp. 413–23.
- H. Kimura, T. Ogawa, M. Kakiki, A. Matsumoto, and F. Tsukihashi: *ISIJ Int.*, 2005, vol. 45, pp. 506–12.
- H. Matsuura, M. Jurashige, M. Naka, and F. Tsukihashi: *ISIJ Int.*, 2009, vol. 49, pp. 1283–89.